Transparent, near-infrared organic photovoltaic solar cells for window and energy-scavenging applications

Richard R. Lunt[1,2,a)] and Vladimir Bulovic[1,b)]

[1]*Department of Electrical Engineering and Computer Science, Massachusetts Institute of Technology, Cambridge, Massachusetts 02139, USA*
[2]*Department of Chemical Engineering and Materials Science, Michigan State University, East Lansing, Michigan 48824, USA*

We fabricate near-infrared absorbing organic photovoltaics that are highly transparent to visible light. By optimizing near-infrared optical-interference, we demonstrate power efficiencies of $1.3 \pm 0.1\%$ with simultaneous average visible transmission of $>65\%$. Subsequent incorporation of near-infrared distributed-Bragg-reflector mirrors leads to an increase in the efficiency to $1.7 \pm 0.1\%$, approaching the $2.4 \pm 0.2\%$ efficiency of the opaque cell, while maintaining high visible-transparency of $>55\%$. Finally, we demonstrate that a series-integrated array of these transparent cells is capable of powering electronic devices under near-ambient lighting. This architecture suggests strategies for high-efficiency power-generating windows and highlights an application uniquely benefiting from excitonic electronics. © *2011 American Institute of Physics*. [doi:10.1063/1.3567516]

The low energy density of solar illumination necessitates deployment of solar technologies over large surface areas in order to capture enough of the sun's energy to offset a significant portion of nonrenewable energy consumption. The obstacle of large-area deployment could be overcome with development of a low-cost,[1] transparent, photovoltaic (PV) technology that can be integrated onto window panes in homes, skyscrapers, and automobiles, enhancing the functionality of already utilized transparent surfaces. Presently, window glass used in automobiles and in architectural installations is typically 70%–80% and 55%–90% transmissive, respectively, to visible light,[2] with the reduction in light transmission purposely introduced in the form of absorptive or reflective tinted windows. The additive transparent PV technology can similarly modify the glass transparency, but the nontransmitted light would be utilized for power generation. Although there may be opportunities for inorganic semiconductors in such PV applications, their limited mechanical flexibility, high module cost and, more importantly, the bandlike absorption spectrum limits their potential utility to transparent solar cells. In contrast, the excitonic character of organic and molecular semiconductors results in absorption spectra that are highly structured with absorption minima and maxima that is uniquely distinct from the band-absorption of their inorganic counterparts. Previous efforts to construct semitransparent devices have focused on the use of thin active layers (or spatially segmented films) with light absorption focused in the visible spectrum and therefore have been limited to either low efficiencies <1% (Refs. 3 and 4) or low average visible-light transmissivity (AVT) of 10%–35%,[5–8] since both parameters cannot be simultaneously optimized. In this letter we demonstrate heterojunction organic PV (OPV) cells utilizing a molecular organic donor, chloroaluminum phthalocyanine (ClAlPc), and a molecular acceptor, C_{60}, that show peak-absorption in the ultraviolet and near-infrared (NIR) (wavelength span of $\lambda = 650–850$ nm). Combining the OPVs with selective high-reflectivity near-infrared mirror coatings we optimize device performance while also permitting high transmission of visible photopic light[9] through the entire device.

The OPVs are fabricated on glass substrates that were precoated with 150 nm thick, patterned indium-tin oxide (ITO) transparent anode with 15 Ω/sq sheet resistance (from Kintec Co.), ClAlPc (from TCI), and C_{60} (from Sigma-Aldrich, sublimed) were purified once by vacuum train sublimation prior to loading, while bathocuproine (BCP, from Lumtec) and MoO_3 were used as purchased. MoO_3 (20 nm), ClAlPc (15 nm), C_{60} (30 nm), BCP (7.5 nm), and a 100 nm thick Ag cathode were sequentially deposited via thermal evaporation at a rate of 0.1 nm/s. For the transparent devices, ITO cathodes were rf-sputtered directly onto the organic layers at a deposition rate of 0.005–0.03 nm/s at a low operating power of 7–25 W, with 10 SCCM (SCCM denotes cubic centimeter per minute at STP) Ar flow and sputtering chamber pressure of 6 mTorr. The cathode films were deposited through a shadow mask for single devices, defining a 1 mm $\times$ 1.2 mm active device area; series-integrated OPV cells were grown monolithically via 3-mask procedure to create anode-to-cathode connections of 12 subcells (0.7 cm^2 total active area). A distributed Bragg reflector (DBR) utilized as the transparent NIR mirror[10] was grown separately on quartz substrates via sputtering of seven alternating layers of TiO_2 and SiO_2 at the rate of 0.1 nm/s, with layer thickness selected to form a stop band centered around $\lambda = 800$ nm. Broad-band antireflection (BBAR) coatings[10] (from Knight Optical) precoated on their own quartz substrates (1-side) were attached to the DBR and substrate glass via index matching fluid. Transmission data of the assembled devices were obtained at normal incidence with a Cary Eclipse 5000 dual-beam spectrophotometer without reference samples. Current density versus voltage (*J-V*) characteristics were measured under simulated AM1.5G solar illumination corrected for solar spectrum mismatch. The mismatch factor[11]

---

a)Electronic mail: rlunt@msu.edu.
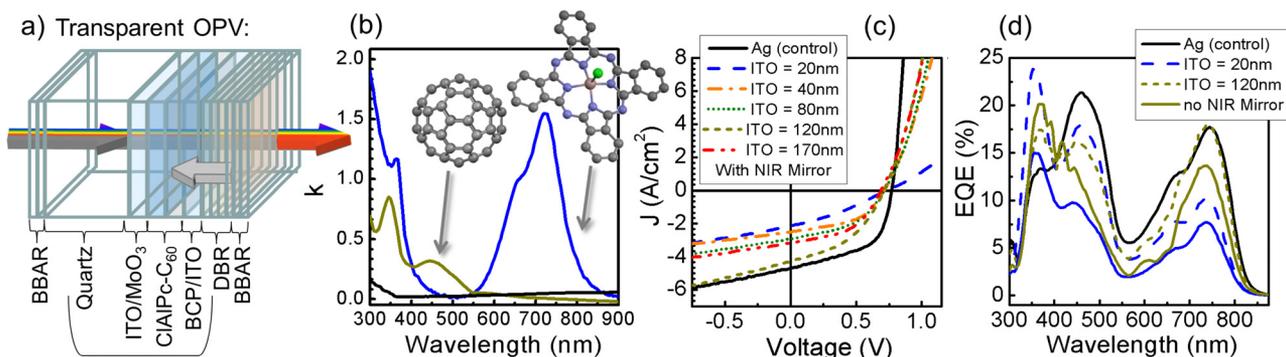b)Electronic mail: bulovic@mit.edu.

FIG. 1. (Color online) (a) Schematic of the transparent photovoltaic architecture. The simple transparent structure without the NIR reflector (ITO-only) is highlighted with the bracket. (b) Imaginary part of the complex index of refraction, k, for the active layers with the molecular structures inset: the ClAlPc donor, C_{60} acceptor, and sputtered ITO (black line) cathode. (c) J-V curves measured under 0.8 sun illumination and (d) EQE for the control cell and for the transparent devices with the NIR reflector as a function of ITO cathode thickness.

was determined to be 0.81 so that the equivalent intensity under testing was ~0.8 sun (see Ref. 12). External quantum efficiency (EQE) measurements were collected utilizing an NREL calibrated mc-Si detector. Optical-interference modeling was carried out according to the method of Ref. 13.

Figure 1(a) shows a schematic of the full transparent solar cells. The imaginary part of complex index of refraction, k, of the active layers is shown in Fig. 1(b), along with the J-V curves for the ClAlPc-C_{60} control and transparent cells in Fig. 1(c). Because the absorption peak for ClAlPc is positioned in the NIR ($\lambda \sim 740$ nm), incorporation of a NIR reflecting mirror enables simultaneous optimization of the solar cell performance and visible-transmissivity as diagramed in Fig. 1(a). The control device with a thick Ag cathode exhibits a power conversion efficiency (η_p) of $2.4 \pm 0.2\%$, open circuit voltage $(Voc)=0.80 \pm 0.02$ V, short-circuit current density $(Jsc)=4.7 \pm 0.3$ mA/cm^2, and fill-factor $(FF)=0.55 \pm 0.03$, which is comparable to previous reports.[14]

Replacing the Ag cathode of the control cell with 20 nm thick ITO cathode, the Jsc drops to 1.5 ± 0.1 mA/cm^2, FF drops to 0.39 ± 0.02, and the Voc decreases slightly to 0.69 ± 0.02 V leading to $\eta_p = 0.5 \pm 0.1\%$. The FF decreases due to an increase in series resistance from the thin ITO cathode that is observable in the J-V curve under forward bias in Fig. 1(c). For thicker (120 nm thick) ITO cathode films, the series resistance diminishes and the FF increases to 0.46, close to the value for the control cell, as shown in Fig. 2. The slight drop in Voc, independent of ITO thickness, is likely due to a change in the cathode-anode work function offset. Nonetheless, it is notable that utilizing ITO as both anode and cathode there is enough deposition anisotropy in the work function to support this large Voc and is likely assisted by the large work function of the MoO_3 layer.[15]

The Jsc decreases as the cathode is switched from Ag to ITO due to the reduced light reflection at the cathode, which reduces the total absorption across the spectrum in the active layers. As the ITO cathode thickness is increased, and the NIR mirror is introduced, the transparent device photocurrent increases threefold, reaching maximum performance for 120 nm thick ITO [see Fig. 2(b)]. Simultaneously, threefold increase in η_p is measured. Modeling the optical modes in these multilayer dielectric stacks, we find a similar trend in the calculated device performance, determined by the interference of the light inside the device with the light reflected from the ITO cathode. Comparing the transmission of the

ITO-only devices in Fig. 3 shows that the absorption for the thinnest ITO cathode (20 nm) and the optimized thicknesses ITO cathode (120 nm) appears equivalent. Inspection of the simulations, however, indicates that the NIR field distribution is shifted from within the ITO anode to the ClAlPc active layer as the ITO cathode thickness increases, so that the total transmission appears the same even though the active layer absorption changes substantially.[12]

Despite the significant impact on the photocurrent, the AVT shows little variation with thickness of the ITO cathode [see Fig. 2(a)]. The optical model predicts AVT values that are in close agreement with experimental data. We note that the high reflectivity of 99% between $\lambda=695$ and 910 nm, also makes these devices useful for simultaneous NIR rejection in architectural cooling. Additionally, the use of the BBAR coatings next to the DBR (outcoupling) and below
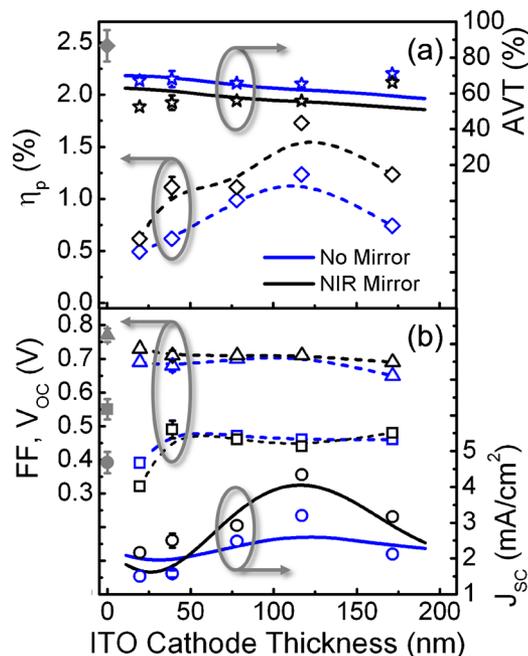

FIG. 2. (Color online) (a) Power conversion efficiency, η_p, (open diamonds), average visible transmission (open stars), (b) open circuit voltage (triangle symbols), fill-factor (square symbols), and short-circuit current (circle symbols) of the transparent devices as a function of ITO cathode thickness with (black symbols) and without (blue symbols) the DBR/BBAR mirror coatings. The control cell performance is included as $x=0$ data (solid gray symbols). Dashed lines are guides to the eyes and solid lines are simulations.
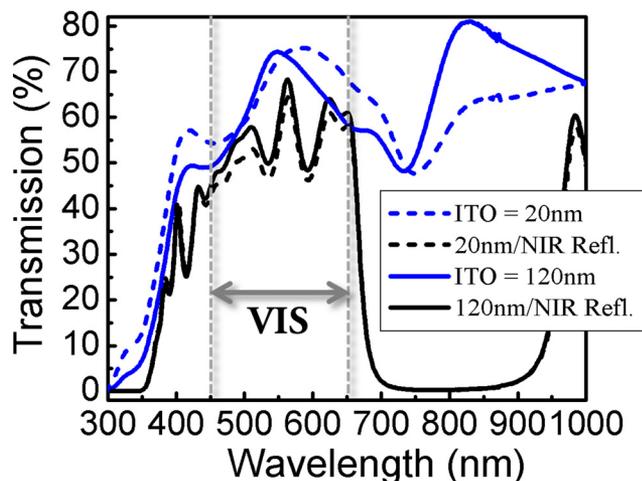
FIG. 3. (Color online) Transmission spectra of the transparent OPV devices for various ITO cathode thicknesses with, and without, the NIR reflector. The approximate visible photopic range is highlighted with vertical dashed-lines. The transmission curves for the assembled transparent OPV closely matches the transmission curve for the NIR mirror (see Ref. 12).

the substrates (incoupling), results in a concomitant increase in the measured AVT by ~4%–6% and the quantum efficiency by ~2%–3%.

To highlight the transparency of the fully assembled device we show the solar cell array in front of a picture of the "Teton mountains" in Fig. 4. Both picture-detail and color-clarity (blue-green) are minimally disrupted so that details of the device array pattern are even difficult to discern. Further, we show that integrating these cells in series, we can power a small liquid crystal display (LCD) clock under near-ambient lighting [see Fig. 4(c)], where the red-white MIT logo can simultaneously be seen through the device.

Optimizing the ITO cathode thickness in the ITO-only devices, we obtain power conversion efficiency of $1.3 \pm 0.1\%$, with a simultaneous AVT of $65 \pm 3\%$. Incorpo-

ration of the NIR reflector and BBAR coatings with the optimized ITO thickness [see Fig. 2(a)], improves the power conversion efficiency to $1.7 \pm 0.1\%$ with an AVT of $56 \pm 2\%$. With the NIR mirror, the increase in the power conversion efficiency stems from additional NIR photocurrent in the ClAlPc layer where the EQE shows a near doubling of the peak ClAlPc EQE from 10% to 18% [see Fig. 1(d)]. Switching from planar to bulk-heterojunctions in these structures or incorporating tandem stacking of subcells with active layer absorption deeper into the infrared,[16] efficiencies of >2%–3% may be possible for this material set with nearly identical visible transmission.

In conclusion, we have demonstrated near-infrared absorbing, transparent planar organic solar cells with a maximum power conversion efficiency of $1.7 \pm 0.1\%$ and average visible transmission of $>55 \pm 2\%$, which is sufficiently transparent for incorporation on architectural glass. Here we exploit the excitonic character of organic semiconductors to produce photovoltaic architectures not easily accessible via inorganic semiconductors. By positioning the active layer absorption selectively in the NIR, we are able to optimize the architecture using a NIR reflector composed of a DBR mirror centered at 800 nm that results in a transparent solar cell efficiency approaching that of the nontransparent control cell. Ultimately these devices provide a guide for achieving high-efficiency and high transparency solar cells that can be utilized in windows to generate power, reduce cooling costs, and scavenge energy.
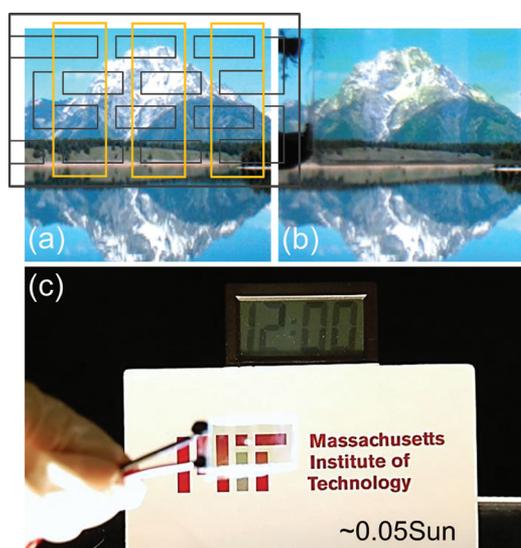
FIG. 4. (Color) (a) Picture of the "Teton mountains" displayed on an LCD screen (b) with the fully assembled transparent solar cell in front of the picture. In (a) the anode/active layer drawing is overlaid on the same picture and the orange boxes highlight the active layer area. (a) and (b) were taken side-by-side during the same exposure. (c) Picture of the series-integrated, transparent cell powering an LCD clock illuminated with ~0.05 sun while allowing for high transparency. See Ref. 12.

[1] J. Kalowekamo and E. Baker, Sol. Energy **83**, 1224 (2009).

[2] C. Tuchinda, S. Srivannaboon, and H. W. Lim, J. Am. Acad. Dermatol. **54**, 845 (2006).

[3] R. F. Bailey-Salzman, B. P. Rand, and S. R. Forrest, Appl. Phys. Lett. **88**, 233502 (2006).

[4] R. Koeppe, D. Hoeglinger, P. A. Troshin, R. N. Lyubovskaya, V. F. Razumov, and N. S. Sariciftci, ChemSusChem **2**, 309 (2009).

[5] R. Kuhn, A. Boueke, A. Kress, P. Fath, G. P. Willeke, and E. Bucher, IEEE Trans. Electron Devices **46**, 2013 (1999).

[6] Q. F. Dong, Y. H. Zhou, J. N. Pei, Z. Y. Liu, Y. W. Li, S. Y. Yao, J. B. Zhang, and W. J. Tian, Org. Electron. **11**, 1327 (2010).

[7] H. Schmidt, H. Flugge, T. Winkler, T. Bulow, T. Riedl, and W. Kowalsky, Appl. Phys. Lett. **94**, 243302 (2009).

[8] J. Meiss, K. Leo, M. K. Riede, C. Uhrich, W.-M. Gnehr, S. Sonntag, and M. Pfeiffer, Appl. Phys. Lett. **95**, 213306 (2009).

[9] Here we define visible light as the region of spectrum where there is photopic response >0.5% of the peak response.

[10] A. Thelen, *Design of Optical Interference Coatings* (McGraw-Hill, New York, 1993).

[11] V. Shrotriya, G. Li, Y. Yao, T. Moriarty, K. Emery, and Y. Yang, Adv. Funct. Mater. **16**, 2016 (2006).

[12] See supplementary material at http://dx.doi.org/10.1063/1.3567516 for solar simulator spectrum and a description of the full circuit assembly.

[13] L. A. A. Pettersson, L. S. Roman, and O. Inganas, J. Appl. Phys. **86**, 487 (1999).

[14] R. F. Bailey-Salzman, B. P. Rand, and S. R. Forrest, Appl. Phys. Lett. **91**, 013508 (2007).

[15] J. Meyer, A. Shu, M. Kroger, and A. Kahn, Appl. Phys. Lett. **96**, 133308 (2010).

[16] I. H. Campbell and B. K. Crone, Appl. Phys. Lett. **95**, 263302 (2009).